Level resolved photoionisation cross sections for Fe I

Smyth, R. T., Ballance, C. P., & Ramsbottom, C. A. (2019). Level resolved photoionisation cross sections for Fe I. *The Astrophysical Journal*, *874*(2), [144]. https://doi.org/10.3847/1538-4357/ab0d25

Published in:
The Astrophysical Journal

Document Version:
Publisher's PDF, also known as Version of record

Queen's University Belfast - Research Portal:
Link to publication record in Queen's University Belfast Research Portal

Publisher rights
Copyright 2019 IOP. This work is made available online in accordance with the publisher's policies. Please refer to any applicable terms of use of the publisher.

General rights
Copyright for the publications made accessible via the Queen's University Belfast Research Portal is retained by the author(s) and / or other copyright owners and it is a condition of accessing these publications that users recognise and abide by the legal requirements associated with these rights.

Take down policy
The Research Portal is Queen's institutional repository that provides access to Queen's research output. Every effort has been made to ensure that content in the Research Portal does not infringe any person's rights, or applicable UK laws. If you discover content in the Research Portal that you believe breaches copyright or violates any law, please contact openaccess@qub.ac.uk.

Download date:04. May. 2023

The Astrophysical Journal, 874:144 (8pp), 2019 April 1 https://doi.org/10.3847/1538-4357/ab0d25
© 2019. The American Astronomical Society. All rights reserved.

Level-resolved Photoionization Cross Sections for Fe I

R. T. Smyth, C. P. Ballance, and C. A. Ramsbottom
Centre for Theoretical Atomic, Molecular, and Optical Physics, School of Mathematics & Physics Queen's University of Belfast, Belfast BT7 1NN, Northern Ireland, UK; rsmyth41@qub.ac.uk, c.ballance@qub.ac.uk, c.ramsbottom@qub.ac.uk
Received 2019 January 31; revised 2019 March 1; accepted 2019 March 4; published 2019 April 2

Abstract

Significant contributions to the UV opacity in the solar atmosphere have been found to stem from bound-free transitions in neutral iron. As such, accurate cross sections for the photoionisation process are required for a detailed and meaningful analysis. However, existing photoionisation cross sections display large discrepancies across the low-energy region, highlighting the need for further calculations. In this work, we present level-resolved photoionisation cross sections for neutral iron across a wide energy range from a 262 level Dirac *R*-matrix calculation. Comparisons with existing experimental measurements reveal good agreement in the positions of the various low-energy resonance features. However, additional comparisons with theoretical data sets highlight wide variations. Significant resonance structures at high photon energies are explored by employing an additional series of 262 level and 896 level Dirac *R*-matrix calculations with a smaller six configuration target. The resulting photoionisation cross sections reproduce the main features from existing experimental observations. The results presented throughout will be useful to those requiring an extensive set of level-resolved photoionisation cross sections for astrophysical applications.

Key words: atomic data – atomic processes – scattering

1. Introduction

The spectra of low ion stages of iron are of vital importance for the interpretation and analysis of astrophysical observations. These species are also some of the main sources of opacity in stellar environments (Basu & Antia 2008; Blancard et al. 2012; Bailey et al. 2014). Neutral iron in particular is found to contribute significantly to the UV opacity in the solar atmosphere (Bell et al. 2001; Castelli & Kurucz 2004) for which a meaningful analysis necessitates the use of accurate photoionisation cross sections (Seaton 1987 and Seaton et al. 1994). However, its complex open 3d atomic structure makes calculations for Fe I extremely challenging, with atomic structures demanding configuration interaction expansions with thousands of fine-structure levels and close-coupling expansions that result in thousands of coupled channels. Despite these difficulties, in an effort to provide high-quality and extensive sets of photoionisation data for Fe I, a number of calculations and experiments of varying sophistication have been carried out.

Early theoretical investigations of Kelly (1972) and Kelly & Ron (1972) made use of many-body perturbation theory, neglecting relativistic effects, and illustrated the importance of correlation effects on the ^{5}D ground-state photoionisation cross section. Subsequent experimental measurements of Tondello (1975) provided absorption spectra of Fe I to allow comparisons with the few available theoretical works. They noted some agreement with the calculations of Kelly & Ron (1972). Further work by Hansen et al. (1977) then provided both an experimental and theoretical investigation into the photoionisation of Fe I. Their relative cross-section measurements were supplemented by Hartree–Fock and intermediate coupling calculations to interpret the observed resonance structures, noting that fine-structure resolved calculations were necessary to obtain more accurate predictions of their observed intensities. Additional measurements of Lombardi et al. (1978) provided an absolute photoionisation cross section. However, this work was limited as they provided a cross section at only a single energy.

Later investigations of Reilman & Manson (1979) calculated total photoionisation cross sections for all atoms and ions with $Z \leqslant 30$ by employing the Hartree–Slater central-field method, noting that agreement within 20% of experiment was expected for the neutral systems such as Fe I. Baluja et al. (1988) then presented an LS-coupled *R*-matrix calculation for the photoionisation of the Fe I ground state. Their calculations included only the lowest ^{6}D, ^{4}F, ^{4}D, and ^{4}P Fe II target terms in the close-coupling expansion and noted that the contributions of resonances converging onto terms above these four target terms may be significant. Despite its limitations, this calculation was a significant step toward larger and more sophisticated *R*-matrix calculations for Fe I such as those of Sawey & Berrington (1990) and Sawey & Berrington (1992). Their calculations, carried out in LS coupling, expanded upon those of Baluja et al. (1988) and considered 17 target terms from the $3d^64s$, $3d^7$, $3d^64p$, and $3d^54s^2$ configurations. In a similar manner to Reilman & Manson (1979), the investigations of Verner et al. (1993) and Verner & Yakovlev (1995) made use of the Hartree–Dirac–Slater central-field method supplemented with simple analytic expressions to fit cross sections for atoms and ions ranging from He to Zn (including Fe I). Although relativistic effects were included in their main calculations, these were omitted from their fitting procedure, only making use of the results averaged over the fine structure.

Additional calculations of Bautista & Pradhan (1995) and Bautista (1997) then employed the LS *R*-matrix method including 52 terms in their close-coupling expansion arising from the $3d^64s$, $3d^54s^2$, $3d^7$, $3d^64p$, and $3d^54s4p$ configurations. In particular, these calculations demonstrated the importance of including the $3d^54s^2$ configuration in the target description, coupling to which resulted in a large enhancement of the ground-state photoionisation cross section. Their results displays several orders of magnitude difference when compared with the results of earlier central-field approximation

calculations. Berrington & Ballance (2001) then investigated the double photoionisation of Fe I by single photon impact by employing the LS *R*-matrix method. In their ground-term photoionisation cross section of Fe I, they presented large inner-shell resonances around four Rydbergs that were previously observed in the experimental investigations of Bruhn et al. (1979), Schmidt et al. (1983), and Feist et al. (1996). However, at lower energies, their cross sections displayed rather large differences when compared with earlier calculations.

Further to the early experimental work of Tondello (1975), Hansen et al. (1977), and Lombardi et al. (1978) are more recent higher-precision measurements of Reed et al. (2009). They provided cross sections for Fe I (in arbitrary units) and noted fair agreement when compared with existing measurements. Most recently, on the theoretical side, Bautista et al. (2017) carried out a significant term-resolved *R*-matrix photoionisation calculation. In their close-coupling expansion, they include the lowest 151 LS terms of Fe II arising from the $3d^6 4s$, $3d^5 4s^2$, $3d^7$, $3d^6 4p$, $3d^5 4p^2$, $3d^5 4s4p$, $3d^6 5s$, and $3d^6 5p$ configurations. They noted an improvement over the earlier term-resolved *R*-matrix calculations of Bautista (1997). Photoionisation cross sections from two additional calculations of Zatsarinny et al. (2017), employing the B-spline *R*-matrix method with 39 terms from the $3d^6 4s$, $3d^5 4s^2$, $3d^7$ configurations and 112 terms from the $3d^6 4s$, $3d^5 4s^2$, $3d^7$, $3d^6 4p$, and $3d^5 4s4p$ configurations, display considerable variations among the low-energy resonance structures when compared with the work of Bautista et al. (2017).

The above review of existing work highlights the need for further steps to resolve discrepancies seen among calculations. It is also apparent that almost all available sets of photoionisation data for neutral iron are term-resolved. To the best of our knowledge, no extensive sets of level-resolved photoionisation cross sections are readily available for neutral iron. The advantage of such a data set has been highlighted in previous photoionisation calculations of Nahar (2002) for C II, Nahar et al. (2010) for O II, and Fivet et al. (2012) for Fe II. They show that models that neglect fine-structure effects may miss additional resonance features due to the presence of fine-structure splitting. Therefore, the motivation for this work is to address the current discrepancies among existing calculations and extend existing LS-coupled photoionisation models to account for the fine structure. This provides an extensive set of level-resolved total and partial cross sections for the ground state and all excited states for use in the accurate modeling of stellar opacities.

The remainder of the paper is arranged as follows. In Section 2.1, we present our Fe II target model, determined using the multiconfigurational Dirac–Fock (MCDF) method, and compare with previous experimental and calculated values. In Section 2.2, we present details and results of our DARC calculations, making use of the parallel Dirac Atomic *R*-matrix Codes (DARC 2019), which have undergone significant development to efficiently handle the present calculations. We extensively compare with existing calculations and also highlight conformity with general features of available experimental data. In Section 3, we present additional DARC calculations using smaller target expansions to explore inner-shell core excited resonance features in the photoionisation cross sections at high energies. Comparisons are made with available experimental and theoretical data. Finally, in Section 4, we draw our conclusions.

2. Photoionisation Calculations

2.1. Target Structure

For our target structure, we adopt the same 20 configuration, 6069 level atomic structure model as presented in our recent work concerning the electron-impact excitation of Fe II, full details of which are given in Smyth et al. (2019). This target model was determined using GRASP^0 (see Dyall et al. 1989 and Parpia & Grant 1991), employing several MCDF calculations along with extended average level procedures to variationally determine the orbitals for our final atomic structure model, which consists of the following set of 20 carefully selected configurations: $3d^7$; $3d^6\{4s, 4p, 4d, 5s, 5p\}$; $3d^5\{4s^2, 4p^2, 4d^2, 4s4p, 5s^2, 5p^2\}$; $3p^5 3d^7\{4s, 4p, 5s\}$; $3p^5 3d^6\{4s^2, 4s5s\}$; $3p^4 3d^9$; $3p^4 3d^8 4s$; and $3p^4 3d^7 4s^2$. When compared with the experimental values of Nave & Johansson (2013), our atomic structure model displays an overall error of 9.3% for the full set of 262 target levels, with average errors of 7.9% and 10.9% for the odd and even parity levels respectively. However, as all existing photoionisation calculations are term resolved, with their target structures optimized in LS coupling, we statistically average our fine-structure levels for a more meaningful comparison. In Table 1, we present a sample of the current GRASP^0 energies (averaged over the fine structure) for the first 30 terms and compare with the term energies given in NIST (2019). In Table 1, we also compare with the recent 35 configuration AUTOSTRUCTURE calculation of Bautista et al. (2017) to give a further indication of the quality of the present 20 configuration GRASP^0 model. When our full set of statistically averaged levels are considered, we see an average error of 10.6%.

2.2. Scattering Calculation and Results

We first note that Dirac *R*-matrix theory for photoionisation is well documented (see Burke 2011) and will therefore be omitted here. For the present DARC calculations, we take forward our complete 20 configuration, 6069 level Fe II target but include only the first 262 levels in the close-coupling expansion. All 262 energies were shifted to coincide with the experimental values of Nave & Johansson (2013). We chose 20 continuum basis orbitals for each value of angular momentum, and we set the *R*-matrix boundary at 19.84 atomic units. These calculations resulted in up to 1788 coupled channels and Hamiltonian matrices of sizes up to 43300×43300. For our final photoionisation cross sections, we employed an energy mesh with a spacing of 2×10^{-4} Rydbergs, spanning 2.5 Rydbergs.

We note that these calculations resulted in a discrepant value for the Fe I ionization potential, yielding a value of 0.734 Ryd compared to the value of 0.581 Ryd reported by Schoenfeld et al. (1995), i.e., a difference of 23%. This overestimation of our ionization potential is a direct result of an over-correlated description of the Fe I system (the *N*-electron Fe II target plus the incident electron). Since all $N+1$ electron correlation functions from the 20 target configurations were determined, the truncation of our 6069 level target at 262 levels ultimately resulted in an excess of correlation effects describing the $N+1$ electron system. However, this difference was remedied by carefully exploring the effects of successively removing

Table 1
Energies of the First 30 Terms of Fe II (in Rydbergs), Relative to the $3d^6(^5D)4s$ ^6D Ground State, from the Current 20 Configuration GRASP^0 Model Compared to the the Recent 35 Configuration AUTOSTRUCTURE Calculation of Bautista et al. (2017)

No.	Config.	Term	NIST	GRASP^0	Bautista17
1	$3d^6(^5D)4s$	^6D	0.00000	0.00000	0.00000
2	$3d^7$	^4F	0.01823	0.02188	0.02933
3	$3d^6(^5D)4s$	^4D	0.07203	0.10916	0.07623
4	$3d^7$	^4P	0.12025	0.10990	0.14407
5	$3d^7$	^2G	0.14272	0.16340	0.17585
6	$3d^7$	^2P	0.16512	0.18244	0.19288
7	$3d^7$	^2H	0.18349	0.20792	0.23547
8	$3d^7$	$^2D2$	0.18605	0.19429	0.20294
9	$3d^6(^3P2)4s$	^4P	0.19141	0.21214	0.23679
10	$3d^6(^3H)4s$	^4H	0.19176	0.22825	0.21300
11	$3d^6(^3F2)4s$	^4F	0.20405	0.23131	0.24070
12	$3d^54s^2$	^6S	0.20692	0.23388	0.19003
13	$3d^6(^3G)4s$	^4G	0.23095	0.26719	0.26329
14	$3d^6(^3P2)4s$	^2P	0.23468	0.27609	0.28181
15	$3d^6(^3H)4s$	^2H	0.23544	0.29130	0.26087
16	$3d^6(^3F2)4s$	^2F	0.24631	0.28387	0.28279
17	$3d^6(^3G)4s$	^2G	0.27465	0.33099	0.30980
18	$3d^6(^3D)4s$	^4D	0.28252	0.31881	0.33161
19	$3d^7$	^2F	0.28707	0.31330	0.34770
20	$3d^6(^1I)4s$	^2I	0.29594	0.35106	0.32597
21	$3d^6(^1G2)4s$	^2G	0.30131	0.33412	0.34088
22	$3d^6(^3D)4s$	^2D	0.32611	0.38262	0.37797
23	$3d^6(^1S2)4s$	^2S	0.33544	0.35314	0.38851
24	$3d^6(^1D2)4s$	^2D	0.34417	0.39518	0.41652
25	$3d^6(^5D)4p$	$^6D^o$	0.34896	0.35601	0.43892
26	$3d^6(^5D)4p$	$^6F^o$	0.38049	0.39960	0.47499
27	$3d^6(^5D)4p$	$^6P^o$	0.38865	0.40440	0.48299
28	$3d^6(^5D)4p$	$^4F^o$	0.40367	0.44718	0.50390
29	$3d^6(^5D)4p$	$^4D^o$	0.40394	0.44718	0.50179
30	$3d^6(^1F)4s$	^2F	0.40556	0.46701	0.47907

configurations of the $N+1$ electron system that were associated with highly excited states of our Fe II target not encapsulated within our close-coupling expansion. For example, it was found that removing all $N+1$ configurations associated with the $3p^53d^74s$, $3p^53d^74p$ and $3p^53d^75s$ target configurations resulted in a slight correction of 0.024 Ryd to the Fe I ionization potential. Going further and removing the $3p^43d^85s$, $3p^53d^64s5s$ and $3p^43d^74s^2$ configurations lead to a further correction of 0.027 Ryd, i.e., an overall correction of 0.051 Ryd.

As an illustration of how the removal of these $N+1$ configurations affects the form of the cross sections, in Figure 1, we present sample photoionisation cross sections from the excited $^5D_1$ level in the ground term, one in which all $N+1$ configurations are included and one in which the $N+1$ configurations associated with the $3p^53d^74s$, $3p^53d^74p$, and $3p^53d^75s$ target configurations are removed. We stress that in both calculations, we are also preserving the accuracy and reliability of the full 20 configuration Fe II target structure. Upon first inspection, it is evident that removing these $N+1$ configurations results in a shift to the left (consistent with a correction to the ionization potential) with little changes to the overall magnitude and shape of the background. However, it is also important to assess the overall impact of these calculations on the dense packs of narrow low-energy resonance structures. Any significant changes in these resonances may be revealed more clearly by looking to the Gaussian convolved cross sections. Therefore, alongside the $^5D_1$ level cross sections in Figure 1, we also present the corresponding convolved cross sections using various widths σ, across the smaller photon energy range that contains the dense packs of resonances to make comparisons clearer. Again, these convolutions reveal that there is a shift of the cross section to the left with little change to the magnitude. There are, at most differences of 2.6%, 2.3%, 6.9%, and 7.9% in the peaks across this 0.25 Ryd energy range for $\sigma = 0.1$, $\sigma = 0.05$, $\sigma = 0.01$, and $\sigma = 0.005$ respectively. When the entire 2.5 Ryd range is considered, we see overall average differences of 1.1% for $\sigma = 0.1$; 1.8% for $\sigma = 0.05$; 6.5% for $\sigma = 0.01$; and 8.4% for $\sigma = 0.005$. These calculations suggest that we can simply shift all cross sections by a fixed amount to correct for the ionization potential. We highlight the fact that despite the discrepancy in the calculated ionization potential the energies of our Fe I levels (presented in Table 2) are in good agreement with NIST values, displaying errors ranging from only 1.5% up to 6.1%.

Given the above considerations and analysis, in Figure 2, we present our final photoionisation cross sections (shifted to correct for discrepancy in the ionization potential as discussed before) from the $3d^64s^2\ ^5D_J$ ($J = 4, 3, 2, 1, 0$) levels in the ground-state complex of Fe I. Alongside this, we also present the ground level cross section from a further 500 level DARC calculation, which has also been shifted to correct for the ionization potential. For this calculation, we use the same 20 configuration target structure described in Section 2.1. This additional calculation serves as a test of the reliability and accuracy of the present 262 level DARC calculation. We see that the results of these 262 and 500 level DARC calculations are very similar, with little changes in shape, magnitude, and positions of resonance structures. In particular, for the background of the cross section, we see at most a difference of approximately 6% between the two calculations.

In Figure 3, we present the cross section from the $^5D_4$ ground level and compare with the relative measurements of Tondello (1975), Hansen et al. (1977), and Reed et al. (2009), normalized so that height the first resonance peak coincides with the present calculations. It is evident that there are rather large variations among these different experimental data sets from threshold up to approximately 0.8 Ryd, making it difficult to arrive at any detailed conclusions about the present calculations. Therefore, it is more appropriate to use these measurements as a guide of the general features in the present cross sections. To a certain extent, we have reproduced the main resonance features revealed by these observations. The first being around 0.654 Ryd, which agrees reasonably well with the observed resonance position at approximately 0.665 Ryd, an error of 1.7%. Another resonance at 0.710 Ryd also agrees very well when compared to the observed position of 0.715 Ryd, an error of 0.7%. Similarly, two closely lying resonances at 0.673 Ryd and 0.679 Ryd agree very well with the observations of Tondello (1975) and Hansen et al. (1977) in terms of position, both displaying errors of only 0.2%, with agreement being closer to the results of Tondello (1975). Two smaller resonance features at 0.613 Ryd and 0.625 Ryd agree excellently with the measurements of Hansen et al. (1977). We also note that the dense pack of resonances near the photoionisation threshold is consistent with the measurements of Reed et al. (2009) while overall agreement with Hansen et al. (1977) is best. A further comparison with the single valued absolute cross section of Lombardi et al. (1978) at 0.592

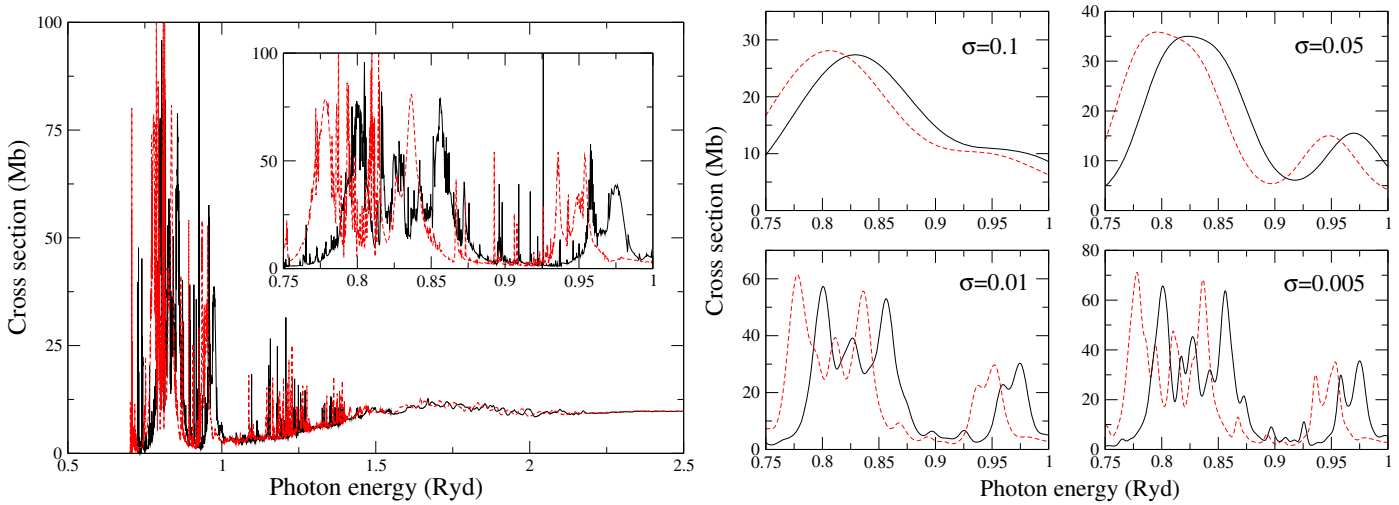

Figure 1. Plot showing sample photoionisation cross sections (left) and Gaussian convolved photoionisation cross sections from the $^5D_1$ level (right). The solid black lines are from calculations with all $N+1$ correlation configurations included and the dashed red lines are from calculations with $N+1$ configurations associated with the $3p^5 3d^7 4s$, $3p^5 3d^7 4p$ and $3p^5 3d^7 5s$ target configurations removed.

Table 2
Energies (in Rydbergs) of Levels within the Ground Term of Fe I Obtained from the Present DARC Calculation, Compared with the Experimental Values given by Nave et al. (1994)

Config.	Term	J	Energy (Ryd)		Error (%)
			Current	Expt.	
$3d^6 4s^2$	^5D	4	0.000000	0.000000	⋯
		3	0.003848	0.003790	1.5
		2	0.006191	0.006415	3.5
		1	0.007895	0.008093	2.4
		0	0.008372	0.008913	6.1

Note. Energies are relative to the $3d^6 4s^2\ ^5D_4$ ground level and errors are given in the final column.

Ryd reveals good agreement. It is interesting to note that the first large resonance peak closest to the ionization threshold appears to agree better with the sharp peaks seen in our excited state photoionisation cross sections presented in Figure 2. This may be due to the thermal excitation of their Fe I sources into the $3d^6 4s^2\ ^5D_J$ ($J = 3, 2, 1, 0$) metastable levels, which lie very close to the $^5D_4$ ground state (see Table 2).

As mentioned in Section 1, nearly all existing photoionisation calculations are in LS coupling. Therefore, to compare, we statistically average our fine-structure cross sections presented in Figure 2. Despite the reasonable agreement with experimental data as presented in Figure 3, there is little agreement with existing calculations, as seen in Figure 4. Comparisons with the early work of Kelly (1972), Reilman & Manson (1979), and Verner et al. (1993) show no agreement in terms of position nor magnitude of the low-energy resonance structures due to the omission of additional complex correlation effects in their calculations. Although agreement in shape improves for photon energies above approximately 0.9 Ryd, there is over a factor of two difference between the magnitude of the backgrounds.

Similarly, comparisons with the work of Berrington & Ballance (2001) and Bautista et al. (2017) reveal a similar picture, with little agreement between the magnitude and positions of the low-energy resonances across the 0.6–0.9 Ryd range. As before, the background of the present cross section is over a factor of two larger at higher energies but there is agreement in shape. Agreement is best when comparing our current statistically averaged cross section with the 112 term calculation of Zatsarinny et al. (2017), showing reasonable conformity in magnitude and position of the resonance features across the low-energy region. Again, agreement in the shape of the background is good but further discrepancies of up to factors of two exist in the magnitude. We do note that toward a photon energy of 2.5 Ryd, the background of the present cross section is in better agreement with the cross sections of Kelly (1972), Reilman & Manson (1979), Verner et al. (1993), and Berrington & Ballance (2001), with at most a factor of approximately 1.3 between them.

We now present a breakdown of the ground-state photoionisation cross section presented in Figure 2. We see from Figures 5(a) and (b) that the bulk of the dense packs of low-energy resonances arise due to photoionisation into the $3d^6 4s$ and $3d^7$ states of the Fe II residual ion, while from Figure 5(c), we see that above approximately 1 Ryd the photoionisation into $3d^5 4s^2$ states of Fe II is the dominant contributor. This accounts for up to 80% of the background of the total cross section above the $3d^5 4s^2$ threshold. From Figure 5(d), we see additional smaller contributions to the background with a slight enhancement of the resonance structures within the 1–1.25 Ryd range due to photoionisation into the $3d^6 4p$ states of Fe II. Furthermore, it can be seen from Figures 5(e) and (f) that contributions to the photoionisation of the ground state into the $3d^5 4s4p$ and $3d^6 5s$ states of Fe II are negligible in comparison.

The data presented here from our 20 configuration, 262 level DARC calculation will be made available to those requiring extensive sets of level-resolved photoionisation cross sections for neutral iron. In the next section, we will go beyond energies of 2.5 Ryd and explore the significant resonance features observed around 4 Ryd.

3. Inner-shell Photoexcitations

Existing experimental investigations (e.g., Bruhn et al. 1979; Schmidt et al. 1983; Feist et al. 1996) and a limited number calculations (e.g., Feist et al. 1996; Berrington & Ballance 2001) have shown large resonances in the photoionisation cross

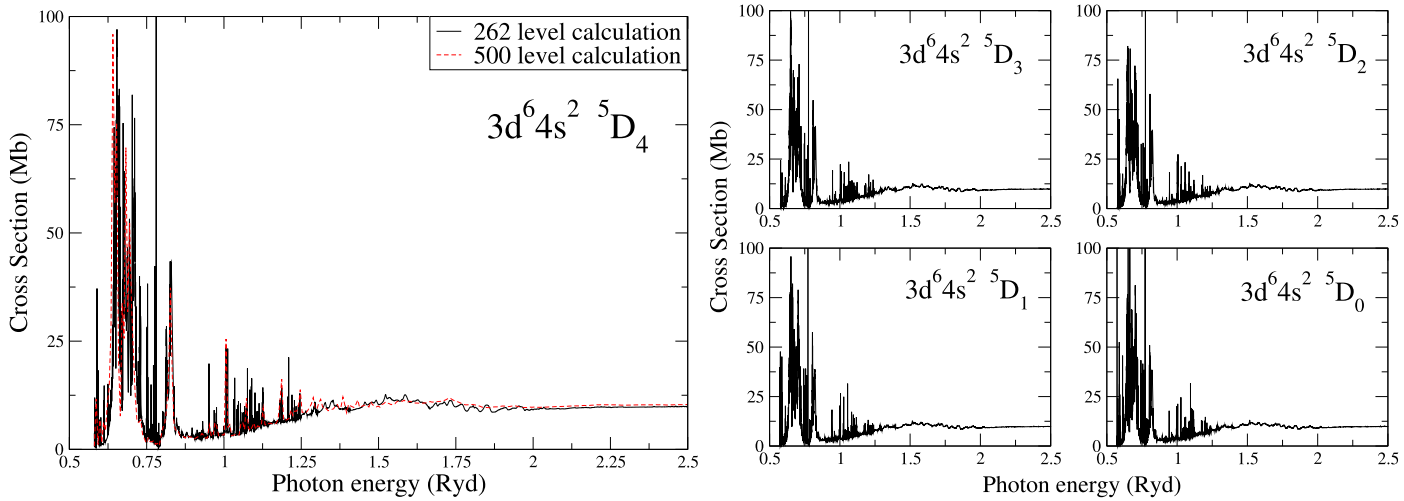

Figure 2. Plot showing the photoionisation cross sections of Fe I from the $3d^64s^2\ ^5D_J$ ($J = 4, 3, 2, 1, 0$) levels in the ground-state complex, obtained from the current 20 configuration, 262 level DARC calculation. The dashed red line in the leftmost plot is the result from the 20 configuration, 500 level DARC calculation.

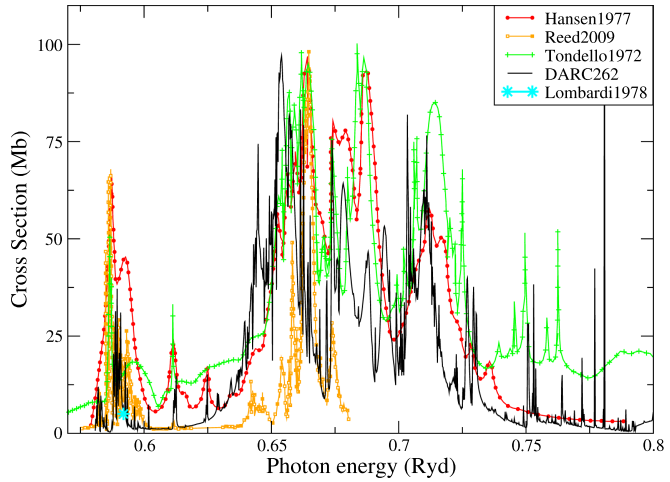

Figure 3. Plot showing the comparison between the $^5D_4$ ground level cross section from the present calculations (solid black line) and existing experimental data sets of Tondello (1975; green plus signs), Hansen et al. (1977; red circles), Lombardi et al. (1978; blue star), and Reed et al. (2009; orange squares).

sections of Fe I around approximately 4 Ryd. These resonances have been attributed to the excitation of a core 3p electron into a vacant 3d orbital, followed by the subsequent emission of a valence 3d electron, i.e.,

$$3p^63d^64s^2 \rightarrow 3p^53d^74s^2 \rightarrow 3p^63d^54s^2\epsilon l. \quad (1)$$

Supported by the analysis of our ground-state photoionisation cross section breakdown in Figure 5, we have supplemented our large 20 configuration 262 level DARC calculation with a series of additional calculations. These included only the $3d^6\{4s, 4p\}$; $3d^5\{4s^2, 4s4p\}$; $3d^7$; and $3p^53d^64s^2$ configurations in the target description. With this smaller six configuration target structure, only 11 continuum orbitals were needed to reach incident energies of up to nearly 9 Ryd, which is sufficient enough to encapsulate the large resonances around 4 Ryd. We note that the purpose of these calculations is not to reproduce experimental observations exactly, but rather to allow us to explore the general features of significant resonance structures at high photon energies.

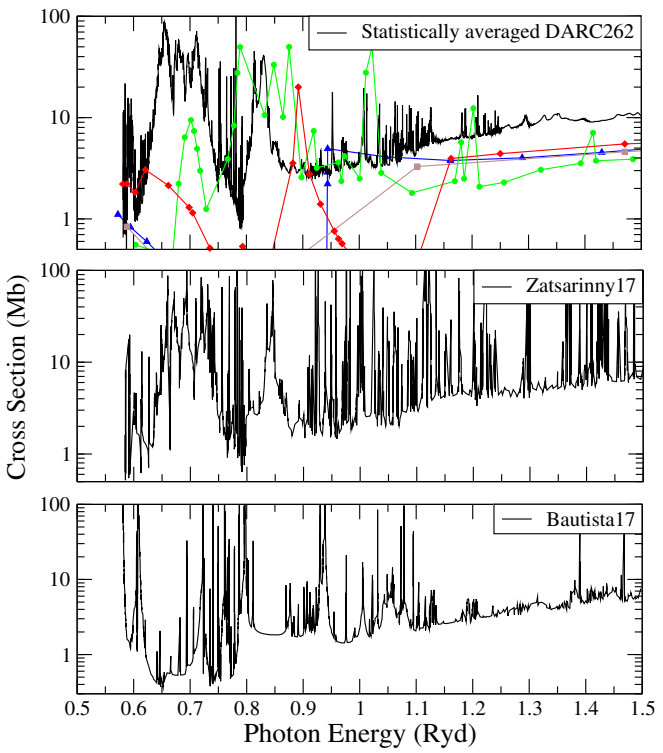

Figure 4. Plot showing the comparison between the current work and existing calculations. The top plot shows the current statistically averaged DARC262 ^{5}D ground-term cross section (solid black line) compared with Kelly (1972; red diamonds), Reilman & Manson (1979; brown squares), Verner et al. (1993; blue triangles), and Berrington & Ballance (2001; green circles). The ground-term cross sections of Zatsarinny et al. (2017) and Bautista et al. (2017) are provided for reference in the middle and lower plots, respectively.

In the top panel of Figure 6, we present cross sections from two calculations retaining the first 262 levels of our target expansion. The first included all $N+1$ configurations associated with our six-target configurations, whereas the second was a reduced calculation in which we removed the $N+1$ configurations associated with the $3p^53d^64s^2$ configuration. Comparing the results from the first calculation with the experimental measurements of Feist et al. (1996) and Bruhn et al. (1979) reveal that we have reproduced the main resonance

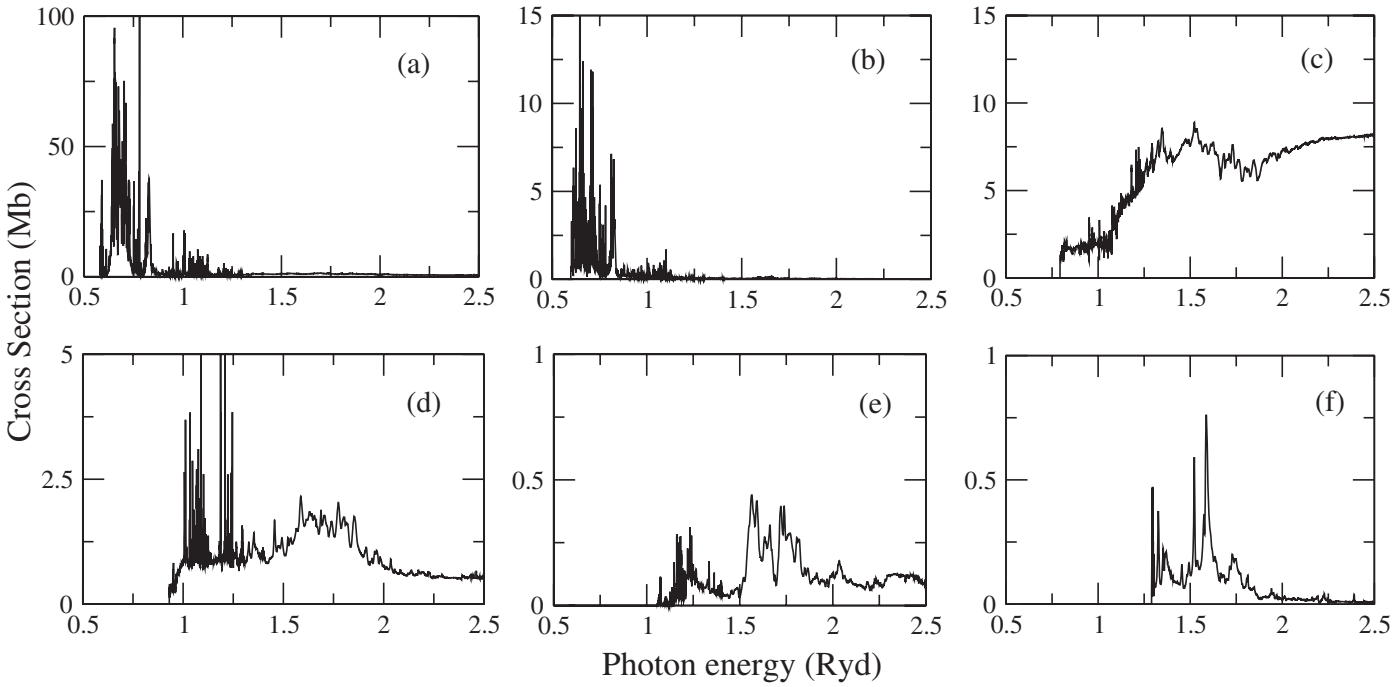

Figure 5. Plot showing the contributions to the $3d^6 4s^2\ ^5D_4$ Fe I ground-state photoionisation cross section. Shown are the partial photoionisation cross sections of the $^5D_4$ ground state into all (a) $3d^6 4s$ states; (b) $3d^7$ states; (c) $3d^5 4s^2$ states; (d) $3d^6 4p$ states; (e) $3d^5 4s 4p$ states; and (f) $3d^6 5s$ states of the residual Fe II ion.

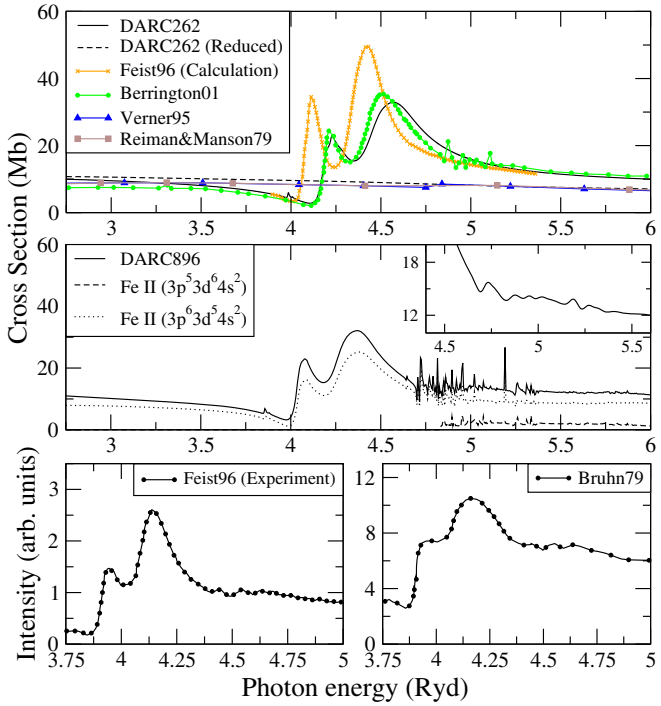

Figure 6. Plot comparing the observed and calculated resonance features at high photon energies. Top row: 262 level DARC (solid black line), reduced 262 level DARC (dashed black line), Berrington & Ballance (2001; green circles), Reilman & Manson (1979; brown squares), Verner et al. (1993; blue triangles), and calculations of Feist et al. (1996; orange crosses). Middle row: 896 level DARC (Solid black line) with partial photoionisation cross sections into only $3d^5 4s^2$ (dotted black line) and $3p^5 3d^6 4s^2$ (dashed black line) states of Fe II. Bottom row: experimental observations of Feist et al. (1996) and Bruhn et al. (1979).

features quite well. Discrepancies in these resonances exist however, with errors in position of approximately 7% and 10% for the first and second peaks, respectively. Comparisons with the calculations of Berrington & Ballance (2001) show very good agreement, with at most a 6.8% difference in the height and a 1.4% difference in the position. Additional comparisons with the calculations of Feist et al. (1996) reveal some disagreement in both height and position of the resonances, with the peaks from the present calculations lying approximately a factor of 1.5 lower and displaying a difference of 3% in position.

From Figure 6, it is evident that the second reduced 262 level DARC calculation does not produce the same resonance structures. This is due to the omission of the $N+1$ configurations associated with our $3p^5 3d^6 4s^2$ target configuration, namely $3p^5 3d^7 4s^2$. Therefore, the Fe I core excitation $3p^6 3d^6 4s^2 \rightarrow 3p^5 3d^7 4s^2$ in Equation (1) cannot be described and no resonance is seen. Instead, we see very good agreement with the results from earlier central-field calculations of Reilman & Manson (1979) and Verner et al. (1993). This is to be expected since central-field-type calculations do not account for the indirect pathways necessary to describe the inner-shell $3p \rightarrow 3d$ excitation in Equation (1). As a result of their omission, the significant resonance structures are absent from the cross sections and agreement with our reduced 262 level DARC calculation is best.

Comparisons with the measurements of Feist et al. (1996) and Bruhn et al. (1979) give us confidence that the resonances displayed in our Figure 6 are physical features. However, as this energy region is well beyond our final 262 level target threshold, we must go further and verify that our calculated resonance structures arise due to the included $N+1$ configurations (demonstrated in the top panel of Figure 6 and discussed in the previous paragraph) and are not pseudo-resonances due to the lack of target description at these energies. For this, we carried out an additional calculation that included all 896 levels from the six-target configurations and included all corresponding $N+1$ configurations. This calculation resulted in up to 6105 coupled channels and Hamiltonian matrices of sizes up to 67242 × 67242. The cross section is

presented in the middle panel of Figure 6, which again shows that we have reproduced the two dominant resonance features along with improvements in the positions, which now agree very well with the calculations of Feist et al. (1996) and displaying only 3% and 5% differences for the first and second peaks, respectively, when compared with experimental observations. A breakdown of our 896 level cross section shows that the main contributor to these resonances is due to photoionisation into $3d^5 4s^2$ states of Fe II, consistent with Equation (1), with additional enhancements to the background due to photoionisation into the $3p^5 3d^6 4s^2$ states of Fe II. We now also have a number of sharp resonance features across the 4.5–5.5 Rydberg range due to the extra 634 levels included in the close-coupling expansion. This is somewhat consistent with a number of small sharp peaks on the decreasing background, which have been seen in the experimental work of Bruhn et al. (1979) and also in the calculations of Berrington & Ballance (2001). Convolving our cross section with a Gaussian of width $\sigma = 0.05$ smooths out the sharp resonances (see the inset in Figure 6) and improves the agreement with experiment.

The above 262 level and 896 level calculations highlight the fact that the presence of the two significant resonance features depends largely on the $N+1$ configurations included in the calculation. However, our calculated resonances can only be considered real when the full set of 896 target levels are explicitly included in the close-coupling expansion. It is apparent that we also benefit from a more complete target description in this resonance region such that overall agreement with experimental observation improves when the $3p^5 3d^6 4s^2$ target states are included in the close-coupling expansion.

4. Conclusions

In this work, we have investigated the photoionisation of Fe I using relativistic methods for both the atomic structure and scattering calculations. Existing data sets, which are almost exclusively in LS coupling, have been extended to include the fine-structure splitting and the results presented here provide extensive level-resolved photoionisation cross sections for Fe I of particular relevance to those requiring data for high-precision astrophysical modeling.

Our accurate Fe II target description was determined from a series of detailed MCDF calculations, with our final atomic structure model consisting of 20 configurations and 6069 fine-structure levels. Comparisons with existing experimental energy level measurements revealed good agreement, giving confidence in the accuracy and reliability of our calculations. This model was then carried through to a substantial 262 level scattering calculation, making use of the recently upgraded and highly optimized versions of the parallel Dirac atomic *R*-matrix codes. Results from our scattering calculations were compared with various experimental measurements that verified the low-energy resonance features produced in our photoionisation cross sections. When compared with existing theoretical data sets, significant differences were seen. However, agreement was best when comparing with an earlier 112 term B-spline *R*-matrix calculation. Further confidence in the accuracy, reliability, and convergence of our results was obtained by carrying out an additional 500 level Dirac *R*-matrix calculation, the results of which agreed very well with our main 262 level calculations.

Aided by a detailed configuration breakdown of our cross sections, additional scattering calculations allowed us to explore significant resonance structures around an incident photon energy of 4 Ryd. The resonance features seen in existing experimental data sets were well reproduced by our calculations. However, discrepancies in the positions of the resonances were seen due to the relatively simple six configuration target structure. The presence of these significant resonances in the cross section was found to depend on the inclusion of $N+1$ states associated with the $3p^5 3d^6 4s^2$ target configuration as opposed to the explicit inclusion of those $3p^5 3d^6 4s^2$ target states in the close-coupling expansion.

The work presented throughout this paper will be of use to those requiring an extensive set of level-resolved total and partial photoionisation cross sections for the ground and excited states for use in astrophysical applications, including the modeling of stellar opacities.

This work is supported by the UK Research and Innovation —Science and Technology Facilities Council grant award ST/P000312/1. All calculations were carried out on the Cray XC40 (Hazel Hen) supercomputer at the High Performance Computing Centre in Stuttgart, on the Cray XC30 supercomputer (ARCHER) at the EPCC in the UK, and on a local computer cluster at Queen's University Belfast.

ORCID iDs

R. T. Smyth https://orcid.org/0000-0002-4359-1408

References

Bailey, J. E., Nagayama, T., Loisel, G. P., et al. 2014, Natur, 517, 56
Baluja, K., Butler, K., Le Bourlot, J., & Zeippen, C. 1988, J. Phys. Colloques, 49, C1
Basu, S., & Antia, H. 2008, PhR, 457, 217
Bautista, M. A. 1997, A&AS, 122, 167
Bautista, M. A., Lind, K., & Bergemann, M. 2017, A&A, 606, A127
Bautista, M. A., & Pradhan, A. K. 1995, JPhB, 28, L173
Bell, R. A., Balachandran, S. C., & Bautista, M. 2001, ApJL, 546, L65
Berrington, K. A., & Ballance, C. 2001, JPhB, 34, L383
Blancard, C., Cossé, P., & Faussurier, G. 2012, ApJ, 745, 10
Bruhn, R., Sonntag, B., & Wolff, H. W. 1979, JPhB, 12, 203
Burke, P. 2011, R-Matrix Theory of Atomic Collisions: Application to Atomic, Molecular and Optical Processes (Berlin: Springer)
Castelli, F., & Kurucz, R. L. 2004, A&A, 419, 725
DARC 2019, R-Matrix Codes, http://connorb.freeshell.org/
Dyall, K., Grant, I., Johnson, C., Parpia, F., & Plummer, E. 1989, CoPhC, 55, 425
Feist, H., Feldt, M., Gerth, C., et al. 1996, PhRvA, 53, 760
Fivet, V., Bautista, M. A., & Ballance, C. P. 2012, JPhB, 45, 035201
Hansen, J. E., Ziegenbein, B., Lincke, R., & Kelly, H. P. 1977, JPhB, 10, 37
Kelly, H. P. 1972, PhRvA, 6, 1048
Kelly, H. P., & Ron, A. 1972, PhRvA, 5, 168
Lombardi, G. G., Smith, P. L., & Parkinson, W. H. 1978, PhRvA, 18, 2131
Nahar, S. N. 2002, PhRvA, 65, 052702
Nahar, S. N., Montenegro, M., Eissner, W., & Pradhan, A. K. 2010, PhRvA, 82, 065401
Nave, G., & Johansson, S. 2013, ApJS, 204, 1
Nave, G., Johansson, S., Learner, R. C. M., Thorne, A. P., & Brault, J. W. 1994, ApJS, 94, 221
NIST 2019, NIST Database, doi:10.18434/T4W30F
Parpia, F. A., & Grant, I. P. 1991, JPhy4, 01, C1
Reed, B., Lam, C.-S., Chang, Y.-C., et al. 2009, ApJ, 693, 940
Reilman, R. F., & Manson, S. T. 1979, ApJS, 40, 815
Sawey, P. M. J., & Berrington, K. A. 1990, JPhB, 23, L817
Sawey, P. M. J., & Berrington, K. A. 1992, JPhB, 25, 1451
Schmidt, E., Schroder, H., Sonntag, B., Voss, H., & Wetzel, H. E. 1983, JPhB, 16, 2961

Schoenfeld, W. G., Chang, E. S., Geller, M., et al. 1995, A&A, 301, 593
Seaton, M. J. 1987, JPhB, 20, 6363
Seaton, M. J., Yan, Y., Mihalas, D., & Pradhan, A. K. 1994, MNRAS, 266, 805
Smyth, R. T., Ramsbottom, C. A., Keenan, F. P., Ferland, G. J., & Ballance, C. P. 2019, MNRAS, 483, 654
Tondello, G. 1975, MmSAI, 46, 113
Verner, D., Yakovlev, D., Band, I., & Trzhaskovskaya, M. 1993, ADNDT, 55, 233
Verner, D. A., & Yakovlev, D. G. 1995, A&AS, 109, 125
Zatsarinny, O., Fernandez-Menchero, L., & Bartschat, K. 2017, Journal of Physics: Conference Series, 875, 022002